Hyperfine measurement of the 6P$_{1/2}$ state in ^{87}Rb using double resonance on blue and IR transition

Elijah Ogaro Nyakang'o[1] , **Dangka Shylla**[1] , **Vasant Natarajan**[2] and **Kanhaiya Pandey**[1]

[1] Department of Physics, Indian Institute of Technology Guwahati, Guwahati, Assam 781039, India
[2] Department of Physics, Indian Institute of Science, Bangalore, 560012, India

E-mail: kanhaiyapandey@iitg.ac.in

CrossMark

Abstract

In this paper, we present the spectroscopy of the 6P$_{1/2}$ state in ^{87}Rb using a double-resonance technique at 780 nm and 421 nm. The double-resonance technique is implemented using electromagnetically induced transparency (EIT) and optical pumping methods. Using these spectroscopy methods, we have measured the hyperfine splitting of the 6P$_{1/2}$ state with precision of <400 kHz, which agrees well with other spectroscopy methods such as electrical discharge and saturated absorption spectroscopy at 421 nm.

(Some figures may appear in colour only in the online journal)

1. Introduction

Precise measurements of the hyperfine structure of various lines in an atom provide key information about the properties of the nucleus, such as the electric and magnetic moments. Rb is one of the most widely investigated elements in atomic physics for the spectroscopy both experimentally [1–6] and theoretically [7]. This provides great opportunities to verify different methods of theoretical many-body calculations [8, 9]. Hyperfine splitting measurements are good sources of input for studying subjects at the interface of atomic and nuclear physics, such as atomic parity violation [10]. Experimentally, hyperfine structures of 5P$_{3/2}$, 5D$_{3/2}$ and 7S$_{1/2}$ have been measured using single-photon transition 5S$_{1/2}$ → 5P$_{3/2}$ at 780 nm [1–3], and two-photon transitions, 5S$_{1/2}$ → 5D$_{3/2}$ at 778 nm [4] and 5S$_{1/2}$ → 7S$_{1/2}$ at 760 nm [2, 5, 6], respectively.

Besides verifying theoretical calculations, the above referred transitions are used as low-cost optical frequency standards. For example, the precisely measured transition 5S$_{1/2}$ → 5P$_{3/2}$ at 780 nm is used as an optical reference for measuring unknown transitions [3]. All these transitions fall in the IR region;

however, the weak and narrow linewidth ($2\pi \times 1.27$ MHz [11]) transition in the blue region (i.e. at 421 nm) has the advantage of high precision for frequency standards [12, 13] and is a promising candidate for metrology. Measuring the hyperfine splitting of 6P$_{1/2}$ adds important input to theoretical calculations [7]. The hyperfine splitting measurement of 6P states has been carried out using saturated absorption [14] for both 6P$_{1/2}$ and 6P$_{3/2}$ states, or fluorescence spectroscopy [15] for the 6P$_{3/2}$ state on 5S$_{1/2}$ → 6P$_{3/2(1/2)}$ transition, and using RF transition with electrical discharge [16].

The direct detection of absorption of 421 nm on 5S$_{1/2}$ → 6P$_{1/2}$ transition requires heating a Rb vapor cell up to 80 °C–100 °C [14, 17] and using a photodiode with blue enhanced sensitivity. The spectroscopy at 421 nm can also be carried out using double-resonance spectroscopy [18–23], which does not require heating of the Rb vapor cell. The double-resonance method can be the electromagnetically induced transparency (EIT) type in a V-system [24–28], a technique which is known as coherent control spectroscopy (CCS). We have also added an optical pumping technique to the same double-resonance spectroscopy. The precise measurement of the hyperfine interval of the 6P$_{1/2}$ state in ^{87}Rb is carried out using the two double-resonance spectroscopy methods.
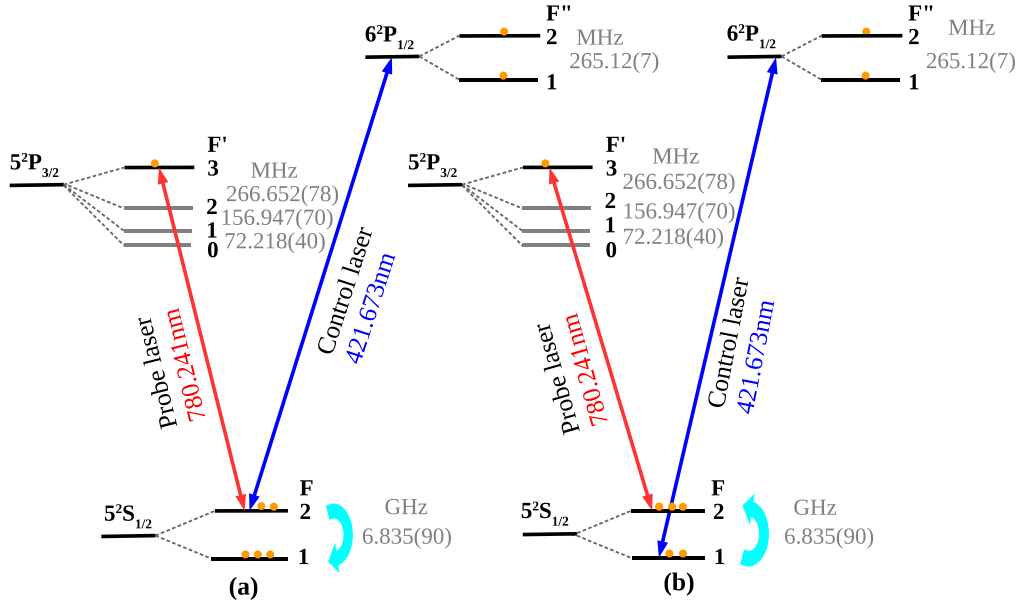
Figure 1. A schematic of a multilevel atomic system interacting with two laser beams in (a) a V-type scheme, and (b) an optical pumping scheme in ^{87}Rb.
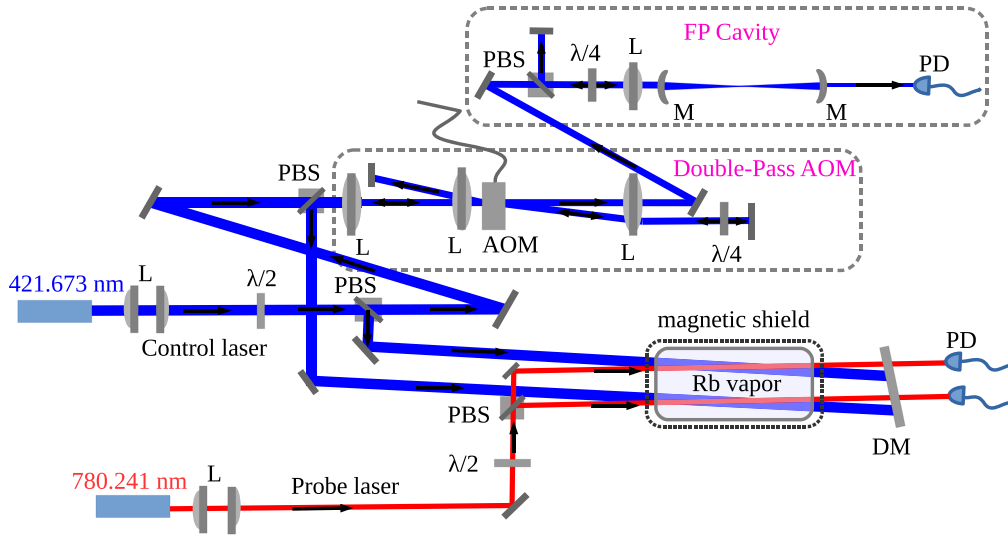
Figure 2. The experimental setup for measuring hyperfine structure using coherent control and optical pumping schemes. L: plano-convex lens; $\lambda/2$: half-wave plate; $\lambda/4$: quarter-wave plate; M: confocal mirror; DM: dichroic mirror; PBS: polarization beam splitter; PD: photodiode; AOM: acousto-optic modulator; FP: Fabry–Perot cavity.

Although the method based upon electrical discharge in [16] provides great precision, it is important to measure hyperfine splitting with different methods to avoid systematic shifts in the experiment due to ion–atom and atom–atom collisions. Similarly, heating the Rb cell also increases atom–atom collision and can cause a collisional/pressure shift [29], which can contribute to systematic shift in the hyperfine measurement.

2. Measurement schemes

2.1. Coherent control scheme

The energy level diagram for the coherent control scheme is given in figure 1(a), and the experimental setup is shown in figure 2. The 780 nm probe laser is locked to resonance on

the $5S_{1/2}(F = 2) \rightarrow 5P_{3/2}(F' = 3)$ cycling transition, and its absorption is monitored as the co-propagating 421 nm control laser beam scans $5S_{1/2}(F = 2) \rightarrow 6P_{1/2}$ transitions. As soon as the 421 nm scanning control laser comes to resonance (i.e. when both laser beams are addressing zero-velocity group atoms), absorption of the 780 nm probe laser is reduced giving rise to a Doppler-free dip. There are two reasons for reduction of the 780 nm probe laser absorption. One is due to the coherent effect, i.e. V-system EIT [25, 28], and another is optical pumping to other ground hyperfine levels, $5S_{1/2}(F = 1)$ [30–32] via $5S_{1/2}(F = 2) \rightarrow 6P_{1/2}$ excitation and $6P_{1/2} \rightarrow 5S_{1/2}(F = 1)$ decay channels. The transparency spectrum is shown in figure 3(a).
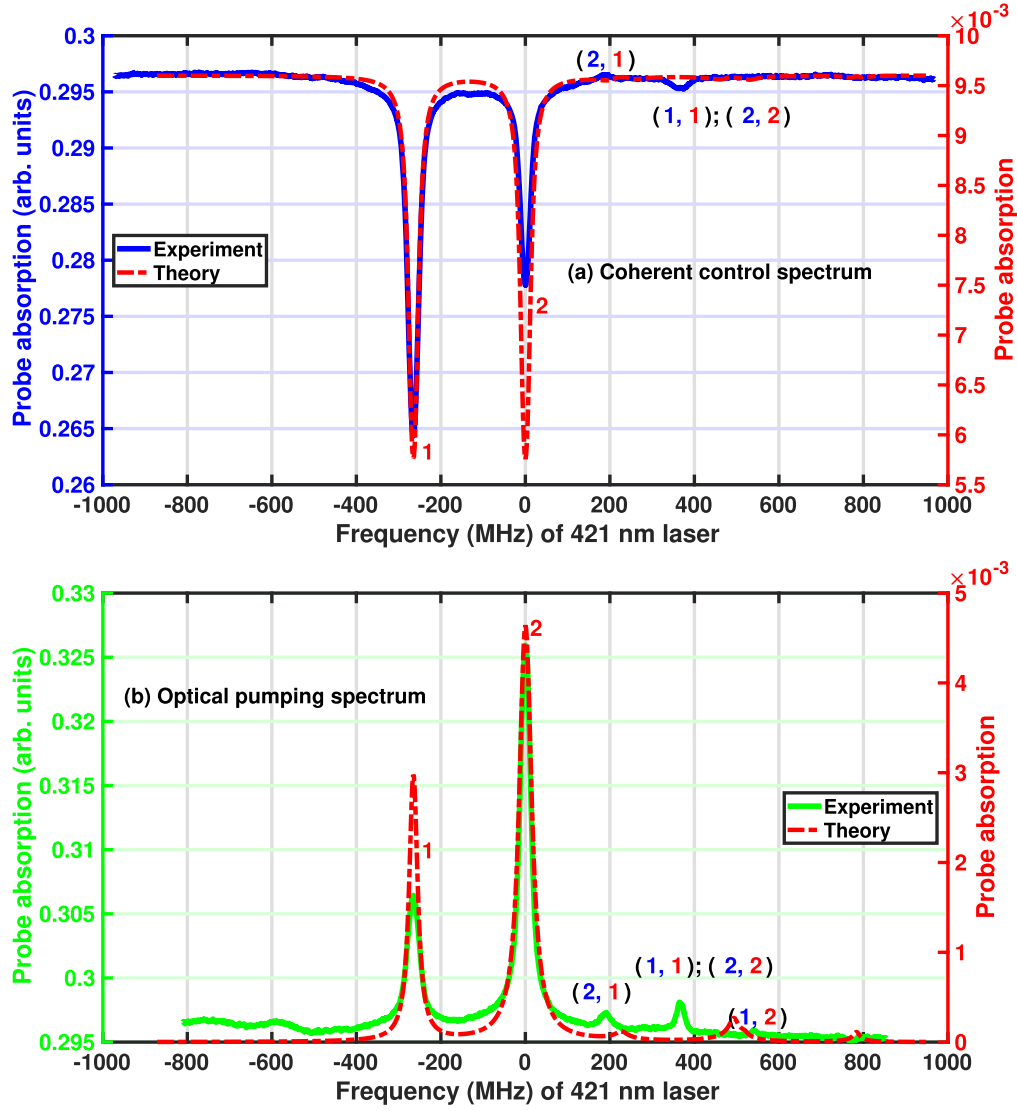
Figure 3. The theoretical and experimental spectrum of $6P_{1/2}$. (a) Coherent control spectrum- a spectrum obtained using coherent control method (b) Optical pumping spectrum- a spectrum obtained using optical pumping method. Extra peaks are caused by atoms moving with velocity 208 m s^{-1} and 330 m s^{-1}, which brings 780 nm and 421 nm lasers to resonance on $5S_{1/2}(F = 2) \leftrightarrow 5P_{3/2}(F' = 1, 2)$ (blue color) and $5S_{1/2}(F = 1(2)) \leftrightarrow 6P_{1/2}(F'' = 1, 2)$ transition (red color).

Besides the two hyperfine peaks due to zero-velocity group atoms, there are other extra peaks outside the main spectrum. The extra peaks are caused by atoms moving with velocities of 208 m s^{-1} and 330 m s^{-1}, respectively. Atoms moving with a velocity of 208 m s^{-1} will see the 780 nm probe laser to be on resonance with the $5S_{1/2}(F = 2) \rightarrow 5P_{3/2}(F' = 2)$ transition. The corresponding two extra peaks are separated by the hyperfine interval of $6P_{1/2}$ and located at 494 MHz from the main peaks, respectively. Similarly, atoms moving with a velocity of 330 m s^{-1} will be resonant for the $5S_{1/2}(F = 2) \rightarrow 5P_{3/2}(F' = 1)$ transition, and another two fold of extra peaks are located at 783 MHz from the main peaks. The theoretical plot in figure 3 is generated using a density matrix calculation for a seven-level system in Doppler-broadened Rb atomic vapors at room temperature (300 K). Due to non-linearity in the scan of the laser, there is a mismatch between experiment and theory in the

position of the extra peaks. The linewidth of the experimental spectrum ranges between 29 and 31 MHz, and the theoretical simulation curve has a linewidth of 26 MHz. However, this linewidth is larger than the natural linewidth (6.065 + 1.27 MHz). This is caused by Doppler mismatch between the 780 nm and 421 nm lasers [33].

2.2. Optical pumping scheme

Figure 1(b) is the energy level diagram for the optical pumping scheme, and the experimental setup is also given in figure 2. The 780 nm probe laser is locked to resonance on the $5S_{1/2}(F = 2) \rightarrow 5P_{3/2}(F' = 3)$ cycling transition and its absorption is monitored as the co-propagating 421 nm control laser beam scans around the $6P_{1/2}$ hyperfine levels on the $5S_{1/2}(F = 1) \rightarrow 6P_{1/2}$ transition instead of the $5S_{1/2}(F = 2) \rightarrow 6P_{1/2}$
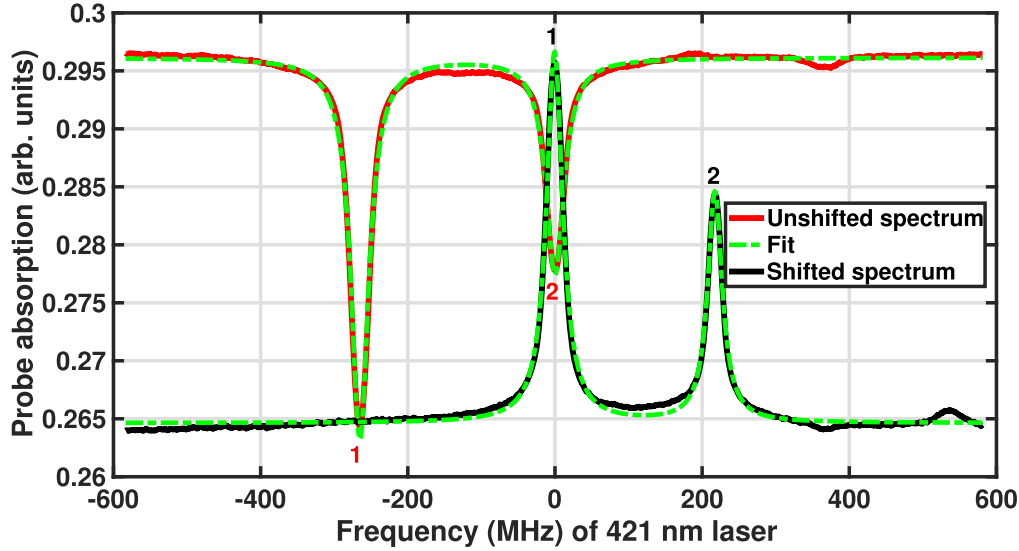
Figure 4. A spectrum of shifted (black color) and unshifted (red color) beams fitted with a Lorentzian line profile (dashed green color) to obtain frequency differences (Δ_{diff}) between the matched peaks.

transition. The 421 nm scanning control laser beam, partially transfers population from the lower ground hyperfine level ($5S_{1/2}(F = 1)$) to the upper ground hyperfine level ($5S_{1/2}(F = 2)$) via $5S_{1/2}(F = 1) \rightarrow 6P_{1/2}$ excitation and $6P_{1/2} \rightarrow 5S_{1/2}(F = 2)$ decay channels. Thus, optical pumping of zero-velocity group atoms to the upper ground hyperfine level [30–32] and the coherence dephasing rate of the ground hyperfine levels [34–36] increase absorption of the probe giving rise to Doppler-free peaks. The absorption spectrum is shown in figure 3(b). Since all velocity group atoms are optically pumped from the $5S_{1/2}(F = 1)$ to the $5S_{1/2}(F = 2)$ ground hyperfine level, extra peaks are formed outside the main spectrum, as explained in the previous section. The linewidth of the experimental spectrum ranges between 29 and 34 MHz, and the linewidth for the theoretical simulation curve is 23 and 34 MHz.

3. Experimental details

3.1. Setup and results

The 780 nm beam is generated from (Thorlabs laser diode L785H1) a home-assembled extended cavity diode laser (ECDL) with typical linewidth of 500 kHz. The error signal for locking the 780 nm laser is generated by frequency modulation using the current of the ECDL at 50 kHz. The error is fed to the piezo using a homemade analog Proportional integral derivative (PID) controller for locking to the particular transition. The 421 nm beam is generated from a commercially available ECDL (TOPTICA, model no. DL PRO HP) with output power of 70 mW and linewidth of <200 kHz. In the experimental setup given in figure 2, the 421 nm laser beam addressing the $6P_{1/2}$ hyperfine level is divided into two laser beams. The first laser beam is passed directly through the Rb vapor cell and co-propagates with one of the 780 nm probe lasers. The second 421 nm laser beam is passed through the acousto-optic modulator (AOM) twice and

its frequency is shifted to be, approximately, the hyperfine interval value. The double-pass AOM configuration has the advantage of preserving the direction of propagation of the laser beam as the frequency of the AOM is changed [37]. The AOM frequency in our double-pass setup is shifted between 130 and 136 MHz. The double-passed AOM beam again passes through the same Rb vapor cell, where it co-propagates with the second 780 nm probe laser. The two sets of co-propagating 421 nm and 780 nm lasers are around 12 mm apart in the same cell. The single-mode operation of the 421 nm laser is monitored using a confocal Fabry–Perot interferometer with free spectral range of 150 MHz. The beam diameter of the 780 nm probe laser is 2×3 mm with measured power of 42 μW (or intensity, I = 1.78 mW cm^{-2}, and corresponding Rabi frequency of $2\pi \times 4.27$ MHz). The beam diameter of the 421 nm control laser is 3×4 mm with measured power of 0.945 mW and calculated intensity, I = 20.05 mW cm^{-2}. The intensity corresponds to a Rabi frequency of $2\pi \times 1.17$ MHz using the dipole moment in [11].

The spectrum of the $5S_{1/2}(F = 2) \rightarrow 6P_{1/2}$ or $5S_{1/2}(F = 1) \rightarrow 6P_{1/2}$ weak transition driven by the 421 nm laser shown in figures 3(a) and (b), respectively, is recorded using a picoscope through the changes in the absorption spectrum of the 780 nm probe laser driving the $5S_{1/2}(F = 2) \rightarrow 5P_{3/2}(F' = 3)$ strong transition. The red and black traces of the experimental spectrum in figure 4 correspond to unshifted and shifted AOM beams, respectively. One of the traces is deliberately inverted to see the matching of the two hyperfine peaks for the shifted and unshifted spectrum. The matching of the peaks is a measure of shifting the frequency of the laser beam by the exact hyperfine interval. The frequency difference (Δ_{diff}) between the two peaks being matched is obtained by fitting the peaks with a Lorentzian line profile (see figure 4) and finding the differences in the peaks' locations. Figure 5 shows a plot of frequency shift ($2 \times$ AOM frequency) versus the frequency difference between the two peaks (Δ_{diff}). The hyperfine interval is obtained using a
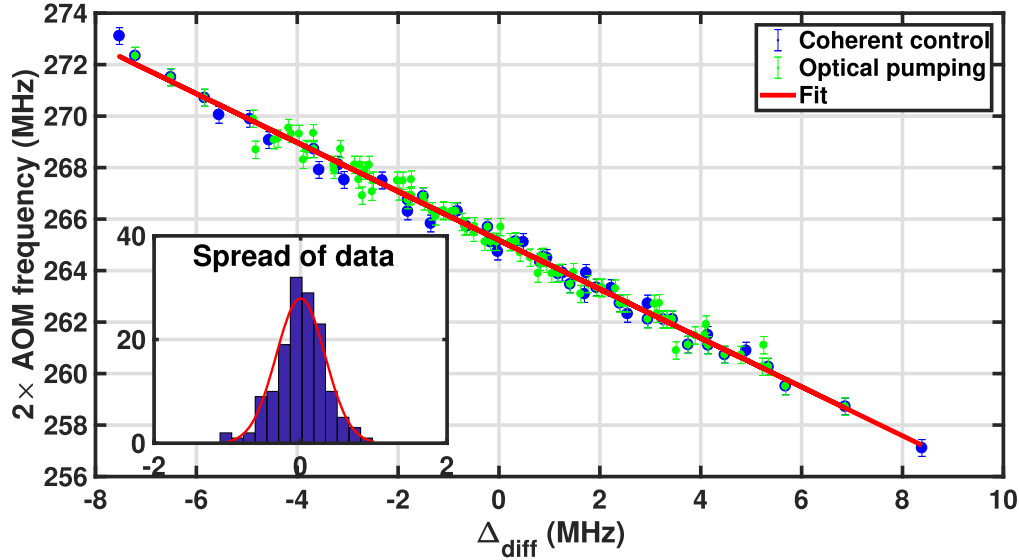
Figure 5. A plot of frequency shift (2 × AOM frequency) versus frequency difference (Δ_{diff}) for the two schemes. The inset shows the spread of data from the mean hyperfine interval.

linear fit on the plot of frequency shift versus Δ_{diff}. The frequency shift corresponding to zero frequency difference ($\Delta_{\text{diff}} = 0$) in the linear fit is the hyperfine interval ($\mathcal{V}_{\text{hfs}}$). This method removes the error due to scan non-linearity, and hence improves the precision of the measurement. From the linear fit the value of $\mathcal{V}_{\text{hfs}} = 265.134 \pm 0.047$ MHz in the case of the coherent control scheme, and $\mathcal{V}_{\text{hfs}} = 265.196 \pm 0.034$ MHz for the optical pumping scheme.

3.2. Errors

3.2.1. Systematic errors.

The main source of the systematic errors is the light shift and stray magnetic field through Zeeman shift. The systematic error arising due to a stray magnetic field is minimized using a μ-metal magnetic shield around the Rb cell. The residual fields are below 1 mG, which corresponds to errors less than 1 kHz. The light shift error is due to presence of the hyperfine levels and the lasers simultaneously driving many levels off resonance causing the light shift of the levels driven resonantly. The locked probe laser $5S_{1/2}(F = 2) \rightarrow 5P_{3/2}(F' = 3)$ cycling transition also drives $5S_{1/2}(F = 2) \rightarrow 5P_{3/2}(F' = 2(1))$ transitions off resonance causing the light shift to the ground state $5S_{1/2}(F = 2)$ upward and excited state $5P_{3/2}(F = 3)$ downwards. However, this shift does not cause any error in the hyperfine interval because it will cause equal shift in the resonance for both the hyperfine levels of $6P_{1/2}$. The scanning control laser is the source of systematic error in the measurement of the hyperfine interval. This is because when it is resonant to $5S_{1/2}(F = 2) \rightarrow 6P_{1/2}(F'' = 1)$, it also drives the $5S_{1/2}(F = 2) \rightarrow 6P_{1/2}(F'' = 2)$ off resonance (negative detuning equal to the hyperfine interval, $\mathcal{V}_{\text{hfs}}$) causing the ground state $5S_{1/2}(F = 2)$ to shift downwards by $\Omega^2/4\mathcal{V}_{\text{hfs}}$. This effect causes resonant frequency for $5S_{1/2}(F = 2) \rightarrow 6P_{1/2}(F'' = 1)$ to be shifted by $+\Omega^2/4\mathcal{V}_{\text{hfs}}$. Similarly, when the control laser is at resonance on the $5S_{1/2}(F = 2) \rightarrow 6P_{1/2}(F'' = 2)$ transition, it is also driving the $5S_{1/2}(F = 2) \rightarrow 6P_{1/2}(F'' = 1)$ transition off resonance (positive detuning equal to the hyperfine interval)

causing the ground state $5S_{1/2}(F = 2)$ to shift upwards by $\Omega^2/4\mathcal{V}_{\text{hfs}}$. This causes the resonant frequency for the $5S_{1/2}(F = 2) \rightarrow 6P_{1/2}(F'' = 2)$ transition to be shifted by $-\Omega^2/4\mathcal{V}_{\text{hfs}}$. The overall light shift errors calculated using the laser intensities in the previous section are 13 kHz and 6 kHz for the coherent control scheme and the optical pumping scheme, respectively.

3.2.2. Statistical error.

The above systematic error is much smaller than the statistical error in the experiment. The non-linear scan of the laser is the main cause of the statistical error. This error is minimized by shifting the AOM frequency within a small range of frequencies around the neighboring hyperfine level. To quantify the statistical error, two traces (shifted and unshifted spectrum) are recorded on two input channels of the picoscope with an average of 20. Three such samples are taken for each AOM frequency, and the spread of the data (Δ_{diff}) is shown by the histogram in the inset of figure 5. The spread of the data gives the statistical error in the experiment and is extracted from the histogram using a Gaussian fit. The extracted statistical error is 0.326 MHz for the coherent control scheme and 0.337 MHz for the optical pumping scheme.

In summary, the statistical error is dominating over systematic errors (light shift and stray magnetic field errors) and fitting errors. The total errors are 0.387 MHz and 0.378 MHz for the coherent control scheme and the optical pumping scheme, respectively. Hence, the hyperfine interval in the coherent control scheme is $\mathcal{V}_{\text{hfs}} = 265.134(373)\{14\}$ MHz and in the optical pumping scheme is $\mathcal{V}_{\text{hfs}} = 265.196(371)\{7\}$ MHz. The measured hyperfine interval is related to the magnetic dipole hyperfine constant, $A = \mathcal{V}_{\text{hfs}}(F \rightarrow F - 1)/F$. The values of A are 132.567(200) MHz and 132.598(200) MHz for the two schemes, respectively. A comparison of the hyperfine interval ($\mathcal{V}_{\text{hfs}}$) and magnetic dipole constant A with earlier works is given in table 1.

J. Phys. B: At. Mol. Opt. Phys. **53** (2020) 095001

E O Nyakang'o *et al*

Table 1. The hyperfine interval ($\mathcal{V}_{hfs}$) and magnetic dipole constant A for the $6P_{1/2}$ state in ^{87}Rb. The number indicated in normal brackets is the statistical plus fitting error, and in curly brackets is the systematic error.

	$\mathcal{V}_{hfs}$ (MHz)	A (MHz)	References
Coherent control	265.134(373){14}	132.567(200)	This work
Optical pumping	265.196(371){7}	132.598(200)	This work
	265.150(460)	132.83(500)	[14]
	265		[38]
		132.56(3)	[16, 39]

4. Conclusions

We have presented two experimental schemes for precision measurement of the hyperfine interval of the $6P_{1/2}$ state of ^{87}Rb, namely coherent control and optical pumping schemes using double resonance at 780 nm and 421 nm. Using an AOM, we have taken care of the scan non-linearity, which is the dominant source of error in the experiment. The measured hyperfine interval is consistent with two other techniques, namely saturated absorption and electrical discharge within the precision of our measurement.

Acknowledgments

ORCID iDs

Elijah Ogaro Nyakang'o ⬤ https://orcid.org/0000-0002-3215-9871

Dangka Shylla ⬤ https://orcid.org/0000-0002-3905-4589

Vasant Natarajan ⬤ https://orcid.org/0000-0002-1456-665X

Kanhaiya Pandey ⬤ https://orcid.org/0000-0002-4154-5694

References

[1] Ye J, Swartz S, Jungner P and Hall J L 1996 *Opt. Lett.* **21** 1280–2

[2] Marian A, Stowe M C, Felinto D and Ye J 2005 *Phys. Rev. Lett.* **95** 023001

[3] Banerjee A and Natarajan V 2004 *Phys. Rev.* A **70** 052505

[4] Touahri D, Acef O, Clairon A, Zondy J J, Felder R, Hilico L, de Beauvoir B, Biraben F and Nez F 1997 *Opt. Commun.* **133** 471–8

[5] Morzyński P *et al* 2013 *Opt. Lett.* **38** 4581–4

[6] Chui H C, Ko M S, Liu Y W, Shy J T, Peng J L and Ahn H 2005 *Opt. Lett.* **30** 842–4

[7] Safronova M S and Safronova U I 2011 *Phys. Rev.* A **83** 052508

[8] Li C B, Yu Y M and Sahoo B K 2018 *Phys. Rev.* A **97** 022512

[9] Safronova M S and Safronova U I 2011 *Phys. Rev.* A **83** 012503

[10] Safronova M S, Budker D, DeMille D, Kimball D F J, Derevianko A and Clark C W 2018 *Rev. Mod. Phys.* **90** 025008

[11] Safronova M S, Williams C J and Clark C W 2004 *Phys. Rev.* A **69** 022509

[12] Zhang S N, Zhang X G, Tu J H, Jiang Z J, Shang H S, Zhu C W, Yang W, Cui J Z and Chen J B 2017 *Chin. Phys. Lett.* **34** 074211

[13] Zhang S, Chang P, Shang H and Chen J 2018 Development of ultra-stable rb-referenced 420 nm optical frequency standard *2018 IEEE International Frequency Control Symposium (IFCS) (IEEE)* pp 1–4

[14] Glaser C, Karlewski F, Grimmel J, Kaiser M, Günther A, Hattermann H and Fortágh J 2019 Absolute frequency measurement of rubidium 5s–6p transitions (arXiv:1905.08824)

[15] Navarro-Navarrete J, Díaz-Calderón A, Hoyos-Campo L, Ponciano-Ojeda F, Flores-Mijangos J, Ramírez-Martínez F and Jiménez-Mier J 2019 (arXiv:1906.07114)

[16] Feiertag D and Zu Putlitz G 1973 *Zeitschrift für Physik A Hadrons and Nuclei* **261** 1–12

[17] Pustelny S, Busaite L, Auzinsh M, Akulshin A, Leefer N and Budker D 2015 *Phys. Rev.* A **92** 053410

[18] Boon J R, Zekou E, Fulton D J and Dunn M H 1998 *Phys. Rev.* A **57** 1323–8

[19] Nishiyama A, Yoshida S, Nakajima Y, Sasada H, Nakagawa K, Onae A and Minoshima K 2016 *Opt. Express* **24** 25894–904

[20] Barnum T J, Grimes D, Zhou Y and Field R W 2015 Double resonance spectroscopy of BaF autoionizing Rydberg states *LXX International Symposium on Molecular Spectroscopy* p TJ06

[21] Ponciano-Ojeda F, Mojica-Casique C, Hernández-Gómez S, López-Hernández O, Hoyos-Campo L M, Flores-Mijangos J, Ramírez-Martínez F, Sahagún D, Jáuregui R and Jiménez-Mier J 2019 *J. Phys. B: At. Mol. Opt. Phys.* **52** 135001

[22] Suzuki M and Yamaguchi S 1988 *IEEE J. Quantum Electron.* **24** 2392–9

[23] Bylicki F, Persch G, Mehdizadeh E and Demtröder W 1989 *Chem. Phys.* **135** 255–65

[24] Banerjee A and Natarajan V 2003 *Opt. Lett.* **28** 1912–4

[25] Das D and Natarajan V 2005 *EPL (Europhys. Lett.)* **72** 740

[26] Das D and Natarajan V 2008 *J. Phys. B: At. Mol. Opt. Phys.* **41** 035001

[27] Das D, Pandey K, Wasan A and Natarajan V 2006 *J. Phys. B: At. Mol. Opt. Phys.* **39** 3111

[28] Menon S and Agarwal G S 1999 *Phys. Rev.* A **61** 013807

[29] Xia W, Dai S Y, Zhang Y, Li K Q, Yu Q and Chen X Z 2016 *Chin. Phys. Lett.* **33** 053201

[30] Feld M S, Burns M M, Kühl T U, Pappas P G and Murnick D E 1980 *Opt. Lett.* **5** 79–81

[31] Smith D A and Hughes I G 2004 *Am. J. Phys.* **72** 631–7

[32] Noh H R 2009 *Eur. J. Phys.* **30** 1181

[33] Urvoy A, Carr C, Ritter R, Adams C S, Weatherill K J and Löw R 2013 *J. Phys. B: At. Mol. Opt. Phys.* **46** 245001

[34] Fulton D J, Shepherd S, Moseley R R, Sinclair B D and Dunn M H 1995 *Phys. Rev.* A **52** 2302–11

[35] Manjappa M, Undurti S S, Karigowda A, Narayanan A and Sanders B C 2014 *Phys. Rev.* A **90** 043859

[36] Tiwari V B, Singh S, Rawat H S, Singh M P and Mehendale S C 2010 *J. Phys. B: At. Mol. Opt. Phys.* **43** 095503

[37] Donley E A, Heavner T P, Levi F, Tataw M O and Jefferts S R 2005 *Rev. Sci. Instrum.* **76** 063112

[38] Grundevik P, Gustavsson M, Rosén A and Svanberg S 1977 *Zeitschrift für Physik A Atoms and Nuclei* **283** 127–32

[39] Arimondo E, Inguscio M and Violino P 1977 *Rev. Mod. Phys.* **49** 31–75